

Analysis of the Heyd-Scuseria-Ernzerhof density functional parameter space

Jonathan E. Moussa,^{1, a)} Peter A. Schultz,¹ and James R. Chelikowsky²

¹⁾ Sandia National Laboratories, Albuquerque, NM 87185, USA

²⁾ Center for Computational Materials, Institute for Computational Engineering and Sciences, Departments of Physics and Chemical Engineering, University of Texas, Austin, TX 78712, USA

(Dated: 23 May 2012)

The Heyd-Scuseria-Ernzerhof (HSE) density functionals are popular for their ability to improve the accuracy of standard semilocal functionals such as Perdew-Burke-Ernzerhof (PBE), particularly for semiconductor band gaps. They also have a reduced computational cost compared to hybrid functionals, which results from the restriction of Fock exchange calculations to small inter-electron separations. These functionals are defined by an overall fraction of Fock exchange and a length scale for exchange screening. We systematically examine this two-parameter space to assess the performance of hybrid screened exchange (sX) functionals and to determine a balance between improving accuracy and reducing the screening length, which can further reduce computational costs. Three parameter choices emerge as useful: “sX-PBE” is an approximation to the sX-LDA screened exchange density functionals based on the local density approximation (LDA); “HSE12” minimizes the overall error over all tests performed; and “HSE12s” is a range-minimized functional that matches the overall accuracy of the existing HSE06 parameterization but reduces the Fock exchange length scale by half. Analysis of the error trends over parameter space produces useful guidance for future improvement of density functionals.

PACS numbers: 31.15.eg,71.15.Mb

I. INTRODUCTION

The exact, nonlocal form for the many-electron Fock exchange energy is known from Hartree-Fock theory. However, it is a standard practice in density functional theory (DFT) to compute this energy by integrating a local energy density per electron that is specified by the local electron density and its derivatives. One of the most popular of these semilocal density approximations is the Perdew-Burke-Ernzerhof (PBE) model¹. Accuracy can be improved by mixing the PBE exchange energy with a fraction of the exact nonlocal Fock exchange energy, producing hybrid functionals such as PBE0². Exchange mixing can also depend on distance: the Heyd-Scuseria-Ernzerhof (HSE) density functional³ retains only short-range Fock exchange and preserves the accuracy of PBE0 while avoiding the cost and pathologies⁴ of long-range Fock exchange. Unlike in traditional Kohn-Sham theory, hybrid functionals generate nonlocal potentials, which is described by a generalized Kohn-Sham (GKS) theory⁵. Ideally, an exact GKS functional can produce both a highest occupied molecular orbital (HOMO) and a lowest unoccupied molecular orbital (LUMO) that have orbital energies equivalent to the negative ionization potential (IP) and electron affinity (EA), respectively. In practice, HSE and other short-range Fock exchange functionals are accurate for band gaps (IP+EA) of semiconductors⁶, but fail significantly for large-gap insulators⁷, molecules⁸, interfaces⁹, and nanostructures¹⁰.

The HSE functional form defines a 2-dimensional space

of DFT functionals³, set by the fraction of Fock exchange, a , at zero electron separation and a length scale, ω^{-1} , on which the short-range Fock exchange is computed,

$$E_{xc}^{\text{HSE}} = aE_x^{\text{HF,SR}}(\omega) + (1-a)E_x^{\text{PBE,SR}}(\omega) + E_x^{\text{PBE,LR}}(\omega) + E_c^{\text{PBE}}. \quad (1)$$

The short-range Fock exchange (in hartrees) is calculated using the spinful Kohn-Sham density matrix $\rho_{\sigma,\sigma'}(\mathbf{r}, \mathbf{r}')$,

$$E_x^{\text{HF,SR}}(\omega) = -\frac{1}{2} \sum_{\sigma,\sigma'} \int d\mathbf{r}d\mathbf{r}' \frac{\text{erfc}(\omega|\mathbf{r}-\mathbf{r}'|)}{|\mathbf{r}-\mathbf{r}'|} \times |\rho_{\sigma,\sigma'}(\mathbf{r}, \mathbf{r}')|^2, \quad (2)$$

while the long-range and remaining short-range exchange are derived from the exchange-hole formulation of PBE¹¹. The intent of HSE was to achieve accuracy equivalent to PBE0, therefore the exchange fraction was limited to its PBE0 value of $a = 0.25$. The HSE06 reparameterization of the HSE form¹² was also based on a variation of ω and not a . The remaining (ω, a) space has been explored only sparsely¹³ with results suggesting that different choices of ω and a improve the accuracy of different physical properties.

HSE is not the first density functional to combine a short-range fragment of Fock exchange with a semilocal model of long-range exchange. The concept has appeared previously as screened exchange (sX) by Bylander and Kleinman¹⁴, where a combination of short-range Fock exchange and the local density approximation (LDA) of correlation and long-range exchange, denoted⁵ sX-LDA, was used to improve LDA band gaps of semiconductors. This application of short-range Fock exchange to band

^{a)} Electronic mail: godotalgorithm@gmail.com

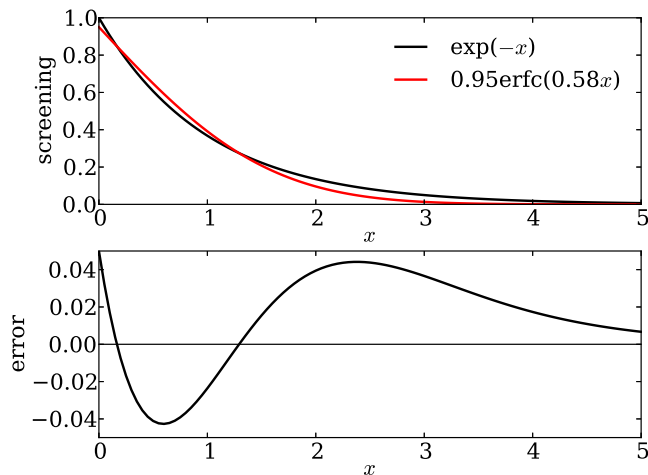


FIG. 1. Approximation of the exponential exchange screening function with a scaled complementary error function. Both functions are displayed in the upper panel and their difference is displayed in the lower panel.

gap estimation is motivated by the Coulomb-hole-plus-screened-exchange (COHSEX) approximation to electron quasiparticle theory¹⁵ in combination with the Thomas-Fermi model of screening. Based on this motivation, an $\exp(-r/r_{\text{TF}})$ screening factor is used in place of $\text{erfc}(\omega r)$ in Eq. (2) and the Fock exchange fraction is set to unity ($a = 1$). The difference in screening form is insignificant, since the two variants can approximate each other,

$$\exp(-x) \approx 0.95\text{erfc}(0.58x), \quad (3)$$

with a maximum pointwise error of ≈ 0.05 (see Fig. 1). However, HSE uses a single ω parameter for all systems, while the r_{TF} parameter in sX-LDA is set to the Thomas-Fermi screening length based on average valence electron density $\bar{\rho}$ (in atomic units),

$$r_{\text{TF}} = \frac{1}{2} \left(\frac{\pi}{3\bar{\rho}} \right)^{1/6}. \quad (4)$$

System-dependence of the Fock exchange length scale is the most important difference between HSE and sX-LDA, especially because $\bar{\rho}$ is not well-defined for a molecule without an arbitrary definition of molecular volume.

Given the flexibility of the HSE form, we fully explore the (ω, a) parameter space to determine if its accuracy and efficiency can be improved further. Also, we assess the variation in results over this space to explain why HSE is accurate and reveal its unresolved shortcomings. First, we search for a “sX-PBE” functional in HSE space that reproduces the performance of sX-LDA, which we define by setting $a = 0.95$ and optimizing ω for band gap estimation. Despite the use of a system-independent ω instead of a system-dependent r_{TF} , sX-PBE is able to surpass the accuracy of sX-LDA. This can be explained by the small degree of variation in r_{TF} values. Next, we search for a “HSE12” parameterization that minimizes

the overall error over multiple test sets. The result is a modest improvement over the HSE06 parameterization, which comes from using a larger Fock exchange fraction ($a = 0.313$). Finally, we search for a range-minimized “HSE12s” parameterization that minimizes the value of ω^{-1} while preserving the accuracy of HSE06. This results in reduction of ω^{-1} by a factor of two, which can reduce the cost of evaluating Eq. (2) by reducing the number of ρ off-diagonals that need to be computed to achieve a target accuracy. After evaluating multiple tests sets, we observe significantly different behavior in two quantities: molecular IPs and EAs as approximated by HOMO and LUMO energies. We can explain this phenomenon as a fundamental limitation of the HSE functional form that results from the use of an environment-independent and homogeneous screening of exchange that is unable to account for inhomogeneous screening environments.

II. COMPUTATIONAL DETAILS

The analysis we present in this paper is based on DFT calculations of isolated molecules and periodic solids. All molecular calculations are performed in GAUSSIAN 09¹⁶. All periodic solid calculations are performed in a modified version of VASP 5.2^{17–21}. All final computational results not directly reported in the paper, as well as all molecular and crystal structures used in this study, are compiled in the supplementary material²¹.

All GAUSSIAN calculations are performed using the 6-311++G(3df, 3pd) basis set, consistent with previous HSE studies¹². The exchange hole form of PBE¹¹ that is used within HSE is applied to all calculations, even when $\omega = 0$. Default settings are used except for the fraction of non-convergent calculations, which we fix by switching to the quadratically-convergent self-consistent field (SCF) method.

All VASP calculations are performed using the manual-recommended PBE projector augmented wave (PAW) pseudopotentials²² with their default planewave basis sets, which are assumed to be transferrable to all DFT functionals considered in this paper. The Brillouin zone integration is performed with the tetrahedron method on a Γ -centered grid, $12 \times 12 \times 12$ for cubic solids and $12 \times 12 \times 8$ for hexagonal solids. The Fock exchange is down-sampled by half in each direction, consistent with convergence studies²³. Fully sampled Fock exchange is applied as an additional perturbative correction to the band gap²⁴. Minor modifications to the current version of VASP are required to calculate the 3 sX-LDA variants considered in this paper²¹.

Comparing DFT results to experiments may require finite temperature and quantum nuclear corrections that are not typically included within DFT itself. The largest corrections occur for formation energies. We account for these corrections at the level of G3 theory for the G3/99 test set²⁵, but omit them for all other test sets. As DFT becomes more accurate, the importance of accounting for

these effects to correctly assess accuracy will grow. Also, spin-orbit coupling is omitted from all calculations. This can have a large effect on band gaps, but the SC/40 test set⁶ that we utilize has removed large spin-orbit effects from its experimental values.

Error distributions are quantified using the mean error (ME) with a (theory - experiment) sign convention, the mean absolute error (MAE), and the root-mean-square error (RMSE). Figures show MAE, which is at present the preferred error average in quantum chemistry.

III. RESULTS AND DISCUSSION

The physically relevant region of the HSE parameter space is $0 \leq \omega \leq \infty$ and $0 \leq a \leq 1$. For sampling and visualization purposes, the ω parameter is mapped to a bounded and dimensionless range separation parameter,

$$\tilde{\omega} = \frac{2}{\pi} \arctan\left(\frac{\omega}{\omega_{\text{HSE06}}}\right), \quad (5)$$

with $\omega_{\text{HSE06}} = 0.208 \text{ \AA}^{-1}$ and $0 \leq \tilde{\omega} \leq 1$. This aligns the HSE06 parameterization to the center of the range separation axis, $\tilde{\omega}_{\text{HSE06}} = 0.5$. All points in HSE space are specified as $(\tilde{\omega}, a)$ ordered pairs. In some cases, the range separation parameter is given as a screening length, which we derive using Eq. (4) as $r_{\text{TF}} = 0.58/\omega$.

A mixture of molecular and bulk solid tests are used to assess the accuracy of HSE functionals. The SC/40 set⁶ contains 33 band gaps and 42 lattice constants of binary and elemental semiconductors (lattice constants of the 3 hexagonal structures are omitted from our study). The G3/99 set²⁶ contains 223 formation energies, 86 IPs, and 58 EAs for small molecules (excited states of SH_2^+ and N_2^+ are omitted from our study). The BH42/04 set²⁷ contains 39 distinct barrier heights mostly for pairwise interactions between small molecules. The T-96R set²⁸ contains 96 bond lengths of small molecules. All of these test sets have been used before to assess the accuracy of HSE functionals^{6,12,13}.

A. SC/40 band gaps

The comparison between sX-LDA and HSE is confined to the SC/40 band gaps because most sX-LDA studies have focused on band structures. We connect sX-LDA to HSE through a sequence of four functional modifications with the results shown in Table I. In sX-LDA, the long-range exchange energy is computed from integration of a globally-weighted local exchange energy density (LDA_G),

$$E_x^{\text{LDA}_G, \text{LR}} = \int d\mathbf{r} \rho(\mathbf{r}) \epsilon_x^{\text{LDA}}[\rho(\mathbf{r})] f\left(\bar{\rho}^{1/3} r_{\text{TF}}\right). \quad (6)$$

The use of $\bar{\rho}$ instead of $\rho(\mathbf{r})$ in the weight function f was initially chosen based on improved band gaps of silicon¹⁴. f is based on an exchange-hole formulation of LDA, and

TABLE I. Comparison of r_{TF} (from Eq. (4), without semicore d -states in $\bar{\rho}$) and band gaps of the SC/40 set⁶ using 5 sX-DFT functionals described in the text, labelled by their exchange-correlation model, screening function, and screening length.

Solid	$r_{\text{TF}}(\text{\AA})$	LDA _G	LDA _L	LDA _L	PBE	PBE	Expt. band gap (eV)
		exp r_{TF}	exp r_{TF}	erfc r_{TF}	erfc r_{TF}	erfc 0.787	
		sX-DFT band gap (eV)					
C	0.389	5.19	4.44	4.27	4.37	5.45	5.48
Si	0.479	1.34	0.74	0.64	0.73	1.08	1.17
Ge	0.489	0.06	0.31	0.36	0.47	0.90	0.74
SiC	0.430	2.52	1.62	1.47	1.56	2.25	2.42
BN	0.391	6.01	4.82	4.62	4.77	6.14	6.22
BP	0.438	2.07	1.41	1.30	1.37	1.88	2.4
BAs	0.450	1.88	1.23	1.17	1.26	1.65	1.46
AlN	0.430	5.29	4.59	4.31	4.47	5.92	6.13
AIP	0.481	2.57	1.78	1.66	1.79	2.22	2.51
AlAs	0.490	2.32	1.58	1.49	1.61	1.98	2.23
AlSb	0.510	1.60	1.15	1.16	1.26	1.50	1.68
GaN	0.441	2.39	1.90	1.68	1.83	3.63	3.50
β -GaN	0.438	2.65	2.12	1.89	2.03	3.32	3.30
GaP	0.480	1.93	1.78	1.66	1.82	2.21	2.35
GaAs	0.489	0.56	0.94	0.99	1.14	1.82	1.52
GaSb	0.508	0.00	0.52	0.61	0.71	1.07	0.73
InN	0.459	1.06	0.13	0.01	0.05	0.95	0.69
InP	0.498	1.35	0.91	0.83	1.01	1.56	1.42
InAs	0.506	0.42	0.11	0.07	0.22	0.73	0.41
InSb	0.524	0.23	0.16	0.17	0.28	0.70	0.23
ZnS	0.479	3.82	2.80	2.59	2.84	3.77	3.66
ZnSe	0.490	2.90	2.05	1.87	2.10	2.91	2.70
ZnTe	0.508	2.44	1.91	1.83	2.00	2.64	2.38
CdS	0.496	2.74	1.67	1.46	1.71	2.46	2.55
CdSe	0.506	2.13	1.21	1.03	1.26	1.92	1.90
CdTe	0.524	1.83	1.24	1.14	1.32	1.84	1.92
MgO	0.422	6.74	5.64	5.17	5.40	7.47	7.22
MgS	0.488	4.67	3.87	3.63	3.92	4.74	5.4
MgSe	0.478	2.78	2.10	1.95	2.06	2.70	2.47
MgTe	0.521	3.12	2.70	2.62	2.82	3.32	3.6
BaS	0.520	3.22	2.41	2.30	2.48	3.00	3.88
BaSe	0.528	2.93	2.16	2.05	2.21	2.66	3.58
BaTe	0.545	2.36	1.68	1.58	1.73	2.04	3.08
ME		-0.24	-0.83	-0.95	-0.80	-0.08	
MAE		0.38	0.83	0.95	0.80	0.28	
RMSE		0.48	0.94	1.08	0.94	0.38	

consistency with the exchange-hole formulation of PBE used in HSE¹¹ requires a local weighting (LDA_L),

$$E_x^{\text{LDA}_L, \text{LR}} = \int d\mathbf{r} \rho(\mathbf{r}) \epsilon_x^{\text{LDA}}[\rho(\mathbf{r})] f\left(\rho(\mathbf{r})^{1/3} r_{\text{TF}}\right). \quad (7)$$

The effect of switching between LDA_G and LDA_L in sX-LDA is shown in the first two sX-DFT columns of Table I. As in silicon, this change results in a systematic band gap

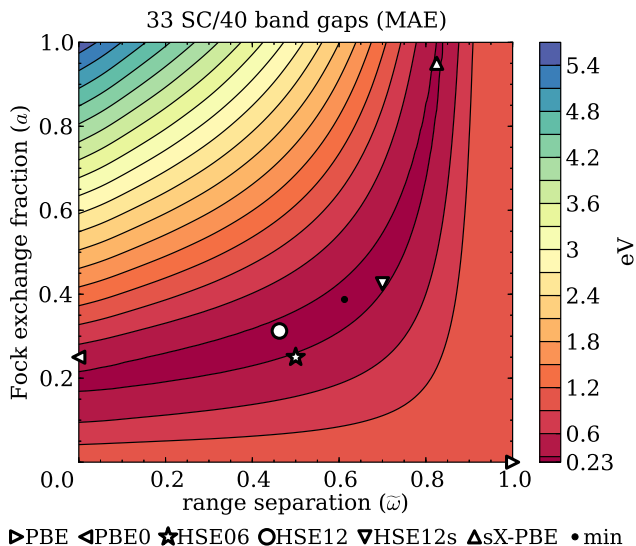


FIG. 2. Semiconductor band gap errors over HSE space. A subset of functionals with approximately equivalent accuracy extend from (0,0.19) to (0.83,1).

underestimation in relation to the more accurate LDA_G. The following two modifications are replacement of the $\exp(-r/r_{\text{TF}})$ screening function with an optimal $\text{erfc}(\omega r)$ approximant as in Eq. (3) and the replacement of the LDA model of correlation and long-range exchange with the PBE model used by HSE. As shown within the third and fourth sX-DFT columns of Table I, this produces small changes in the band gaps. The final modification is to choose a single ω value for all materials to recover the HSE form. The variations in r_{TF} appear to be small because of its sixth-root dependence on $1/\bar{\rho}$ in Eq. (4). As a result, a single optimized ω value is able to surpass the performance of sX-LDA with material-dependent r_{TF} values for this test set. We denote the optimized HSE approximation to sX-LDA as sX-PBE.

The consistency of our results with previous sX-LDA results is mixed. We agree with prior results^{5,14,29,30} on Si but produce significantly smaller band gaps for Ge and GaAs compared to other reported sX-LDA values^{5,29-31}. These discrepancies can be explained by the absence of valence-core interaction terms³² in prior sX-LDA results. The changes are small in Si but large in Ge and GaAs. VASP includes the effect of these missing terms as all-electron corrections within atomic spheres³³.

The MAE of SC/40 band gaps over the whole $(\tilde{\omega}, a)$ HSE space is plotted in Fig. (2). Errors near (1, 0) come from band gap underestimation in the PBE model that is largely attributed³⁴ to the absence of discontinuities in $\delta E_{\text{xc}}^{\text{PBE}}/\delta\rho(\mathbf{r})$. Errors near (0, 1) come from band gap overestimation in Hartree-Fock theory³⁵ (the additional correlation potential has relatively little effect here). In a GKS theory context, the 5 eV error variation in going from (1, 0) to (0, 1) originates from tuning the amount of nonlocality in the GKS potential to compensate for the

lack of $\delta E_{\text{xc}}/\delta\rho(\mathbf{r})$ discontinuities in the semilocal model. Within the HSE space, there is a 1-dimensional subset of similarly good functionals for band gap estimation as judged by MAE. This non-uniqueness is not surprising given that GKS theory introduces greater flexibility in functional form without adding a commensurate amount of new mathematical or physical constraints. Requiring that GKS theory reproduce the exact 1-electron reduced density matrix (1RDM) instead of just electron density can achieve uniqueness³⁶. However, this introduces the ongoing problem of constructing GKS functionals that produce the fractional occupation numbers characteristic of 1RDMs for interacting electrons, even for pure states with an integer number of electrons³⁷.

We can argue for the accuracy of band gaps in HSE based on its similarity to an electron quasiparticle theory. Specifically, the simplification of Hedin's equations using the COHSEX approximation¹⁵ results in the self-energy (assuming a natural spin-dependent extension)

$$\Sigma_{\sigma,\sigma'}^{\text{COHSEX}}(\mathbf{r}, \mathbf{r}') = -\rho_{\sigma,\sigma'}(\mathbf{r}, \mathbf{r}')W_{\sigma,\sigma'}(\mathbf{r}, \mathbf{r}') + \frac{1}{2}\delta_{\sigma,\sigma'}\delta(\mathbf{r} - \mathbf{r}') \left(W_{\sigma,\sigma'}(\mathbf{r}, \mathbf{r}') - \frac{1}{|\mathbf{r} - \mathbf{r}'|} \right) \quad (8)$$

with a non-local sX operator and a local potential derived from the Coulomb hole, both determined by a statically screened Coulomb interaction $W_{\sigma,\sigma'}(\mathbf{r}, \mathbf{r}')$. Minimal, yet realistic, semiconductor screening models³⁸ contain the bulk static dielectric constant ϵ_0 and a Thomas-Fermi-like screening length r_{TF} . A simplified example is

$$W_{\sigma,\sigma'}(\mathbf{r}, \mathbf{r}') \approx \frac{\epsilon_0^{-1} + (1 - \epsilon_0^{-1}) \exp(-|\mathbf{r} - \mathbf{r}'|/r_{\text{TF}})}{|\mathbf{r} - \mathbf{r}'|}, \quad (9)$$

which has a constant Coulomb hole, $(\epsilon_0^{-1} - 1)/(2r_{\text{TF}})$, corresponding to the polarization energy of an electron in a spherical cavity of radius r_{TF} within a dielectric of permittivity ϵ_0 ³⁹. We presume that oversimplification of W breaks the connection between sX and the Coulomb hole, the latter being reasonably approximated by the PBE local potential that corresponds to correlation and long-range exchange.

The position and shape of the 1-dimensional subset of accurate functionals within Fig. (2) can be explained by the connection between HSE and COHSEX. For any one semiconductor, we have one constraint, the band gap, and two free parameters, $(\tilde{\omega}, a)$, therefore each can be fit perfectly along a line in HSE space. The near-overlap of all these lines results from similar parameters for all members of the SC/40 set. The effective W of HSE,

$$W_{\sigma,\sigma'}^{\text{HSE}}(\mathbf{r}, \mathbf{r}') = a \frac{\text{erfc}(\omega|\mathbf{r} - \mathbf{r}'|)}{|\mathbf{r} - \mathbf{r}'|}, \quad (10)$$

can fit Eq. (9) when $r_{\text{TF}}^{-1} = 0$ or $\epsilon_0^{-1} = 0$. We assume similar gap-invariant variations of $(r_{\text{TF}}^{-1}, \epsilon_0^{-1})$ in Eq. (9) from reasonable physical values to $(r_{\text{TF}}^{-1} = 0, \tilde{\epsilon}_0^{-1} > \epsilon_0^{-1})$ or $(\tilde{r}_{\text{TF}}^{-1} < r_{\text{TF}}^{-1}, \epsilon_0^{-1} = 0)$. This explains the optimal $a \approx$

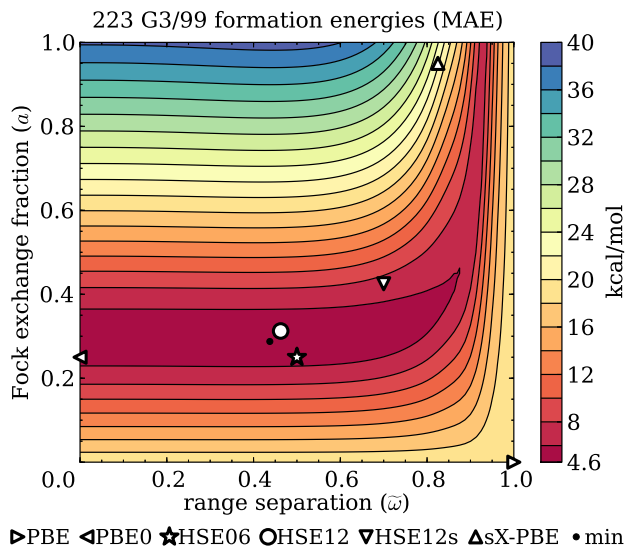


FIG. 3. Molecular formation energy errors over HSE space. A subset of functionals with approximately equivalent accuracy extend from (0,0.3) to (0.93,1).

$\tilde{\varepsilon}_0^{-1} \approx 0.2$ that is larger than the average value for the SC/40 set, $\varepsilon_0^{-1} \approx 0.1$. It also explains the behavior in Table I of an optimal sX-PBE screening length that is longer than the Thomas-Fermi screening lengths. This malleability also explains how the same arguments can be used to support both hybrid⁷ and sX⁵ DFT functionals, with comparable validity and empirical success.

B. G3/99 formation energies

The MAE of G3/99 formation energies over HSE space is shown in Fig. (3). As with the SC/40 band gaps, there is a 1-parameter family of similarly accurate functionals, here with a larger exchange fraction (30% versus 20%) in the hybrid limit and a smaller effective screening length (0.33 Å versus 0.79 Å) in the sX limit. A negligible $\tilde{\omega}$ -dependence for screening lengths larger than 2.4 Å ($\tilde{\omega} \leq 0.55$) shows that the PBE model of long-range exchange performs well beyond that length scale, at least within small molecules. GKS orbitals are only weakly dependent on details of the exchange functional^{40,41}, therefore errors in the exchange functional itself are the main source of MAE variation. In particular, the largest errors occur near (0, 1), where the exact exchange energy is used. This is an example of error cancellation between exchange and correlation models that is often observed in DFT⁴².

The errors in formation energy can be attributed to a systematic bias. Similar to the results for band gaps, the formation energy is underestimated near (1, 0) in Fig. (3) and overestimated near (0, 1), with ME passing through zero near the region of minimal MAE. Here, we use the sign convention of positive formation energies for stable molecules. We observe that the PBE exchange energy

overestimates the Fock exchange energy, $E_x^{\text{PBE}} > E_x^{\text{HF}}$, with larger errors for molecules than for atoms. Also, we observe that the PBE correlation energy underestimates the experimental correlation energy, $E_c^{\text{PBE}} \lesssim E_c^{\text{exp}}$, with errors again larger for molecules than for atoms. These observations are consistent with a cancellation of errors between exchange and correlation contributions to the formation energy.

The similar error trends in Figs. (2) and (3) suggest that HSE functionals are “right for the right reasons”. The ability of HSE functionals to estimate band gaps is explained by quasiparticle theory, which can be extended to cover total energy approximation. This is related to ongoing efforts⁴³ to compute accurate total energies from self-consistent 1-electron Green’s functions. Specifically, the HSE functional can be interpreted as the Galitskii-Migdal formula⁴⁴ applied to the frequency-independent COHSEX self-energy in Eq. (8) to calculate an exchange-correlation energy,

$$E_{\text{xc}} = \frac{1}{2} \sum_{\sigma, \sigma'} \int d\mathbf{r} d\mathbf{r}' \rho_{\sigma', \sigma}(\mathbf{r}', \mathbf{r}) \Sigma_{\sigma, \sigma'}(\mathbf{r}, \mathbf{r}'). \quad (11)$$

The effective HSE self-energy is particularly suited for total energy calculations since it is constrained to exactly reproduce the total energy of the uniform electron gas and PBE gradient corrections thereof.

C. G3/99 ionization potentials and electron affinities

Vertical IPs and EAs can be computed with a GKS functional using either total energy differences between charge states (ΔSCF) or the HOMO/LUMO eigenvalues, if the functional is accurate and free of discontinuities in $\delta E_{\text{xc}}/\delta\rho(\mathbf{r})$. The G3/99 test set contains adiabatic IPs and EAs, which requires the use of relaxed geometries in ΔSCF calculations and a relaxation energy correction for eigenvalue-based vertical excitation energies (the total energy difference of the neutral molecule between neutral and ionized geometries). ΔSCF IPs and EAs are shown in Figs. (4a) and (4d). The variation of errors is smaller than in the formation energies of Fig. (3), which results from increased cancellation of errors because two charge states of a molecule are more similar than a molecule and its dissociated atoms. There is still the same subset-of-accurate-functionals trend, but it does not stand out as strongly without a large background of systematic errors. The eigenvalue-based IP and EA estimates in Figs. (4b) and (4e) show much greater variation over HSE space, comparable to the band gaps in Fig. (2). There is still a subset of accurate functionals, but it is shifted to large Fock exchange fractions ($a \geq 70\%$) that are incompatible with accurate formation energies or band gaps.

The discrepancy between ΔSCF and eigenvalue-based IPs and EAs constitutes both delocalization error⁴⁵ and size-consistency error⁴⁶. Compared to ΔSCF values, the eigenvalues underestimate IP and overestimate EA near

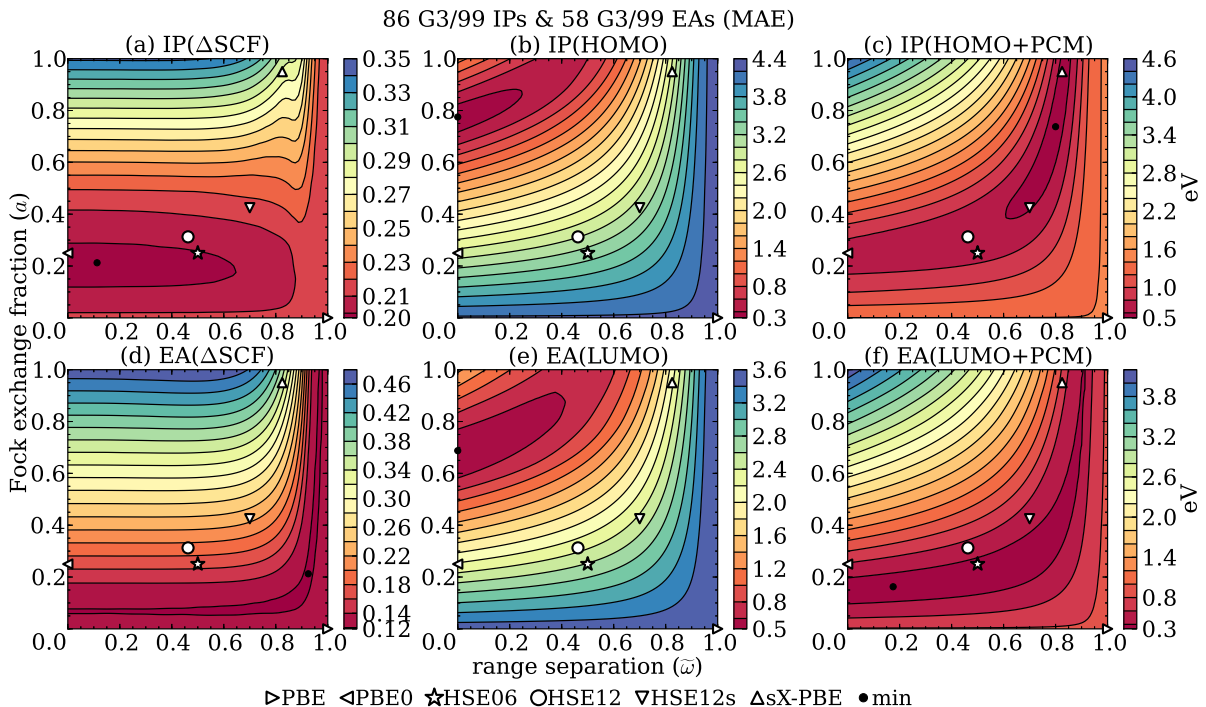


FIG. 4. IP and EA errors in HSE space, comparing Δ SCF to eigenvalue-based estimates and including polarization corrections.

(1, 0) in HSE space and vice versa near (0, 1). If a hole or electron is added to a dilute gas of identical molecules, the charge will delocalize to avoid spurious Coulomb self-interaction and approach the erroneous eigenvalue-based IP/EA for functionals near (1, 0). The opposite effect, localization of charge onto a single molecule, occurs near (0, 1) and forces IP/EA to remain at the more accurate Δ SCF value. This dichotomy is demonstrated in Fig. (5) for a dilute He_n gas with $n = 1, \dots, 20$. DFT functionals with delocalization behavior are not size consistent, and making use of the Δ SCF accuracy requires a single well-defined charge center such as a small molecule or a point defect inside a crystal⁴⁷. The subset of functionals that are accurate for formation energies and band gaps is well within the delocalization regime and uniformly lacks size consistency. In the localization regime, the eigenvalues are no longer equivalent to charge excitations because the localized charges produces nonlinear corrections.

Considering IP as an example, we can account for the difference between Δ SCF and eigenvalue-based estimates with a continued appeal to quasiparticle theory, building on the arguments for band gap accuracy in section III A and total energy accuracy in section III B. For a system X and a DFT functional with a COHSEX-like form, the IP discrepancy can be written as

$$\begin{aligned}
 E(X^+) - E(X) = & -\epsilon_{\text{HOMO}}(X) - \Delta_{\text{relax}} \\
 & + \frac{1}{2} \sum_{\sigma, \sigma'} \int d\mathbf{r} d\mathbf{r}' \left(\frac{1}{|\mathbf{r} - \mathbf{r}'|} - W_{\sigma, \sigma'}(\mathbf{r}, \mathbf{r}') \right) \rho_{\sigma}^+(\mathbf{r}) \rho_{\sigma'}^+(\mathbf{r}')
 \end{aligned}
 \tag{12}$$

by separating orbital relaxation effects Δ_{relax} from terms that assume the cation to have the same W , orbitals, and energies as the neutral system. Within Hartree-Fock theory, the last term vanishes and this is the essential content of Koopmans' theorem⁴⁸, which guarantees that Δ SCF doesn't produce a larger IP than $-\epsilon_{\text{HOMO}}$ since $\Delta_{\text{relax}} \geq 0$. The last term is a polarization correction to the self-interaction of the hole charge ρ^+ and, in an accurate quasiparticle theory, it should cancel Δ_{relax} to produce consistency between IP estimates. If we assume this to be true for a COHSEX model with a realistic W , then errors in HSE can be attributed to the lack of an unscreened Coulomb tail, $W \rightarrow 1/|\mathbf{r} - \mathbf{r}'|$, extending out from a small molecule. The net effect is over-screening in small molecules compared to semiconductors, which is consistent with the offset between Figs. (2) and (4b).

The difference between $1/|\mathbf{r} - \mathbf{r}'|$ and W must originate from an electronically polarizable substance. Since W_{HSE} remains screened even in vacuum, the effect there can be assigned to unphysical vacuum polarization. This error cannot be removed without environment-dependence and inhomogeneity in W_{HSE} , but we can model it by adding comparable errors into Δ SCF calculations. Specifically, we introduce an artificial vacuum polarization into total energies with the polarizable continuum model (PCM)⁴⁹. Over-screening errors of eigenvalue-based IPs and EAs are corrected by subtracting out the errors modeled by the difference between Δ SCF+PCM and Δ SCF values. The results in Figs. (4c) and (4f) are less accurate than Δ SCF values, but they succeed in recovering previous error trends in HSE space. Similar over-screening errors

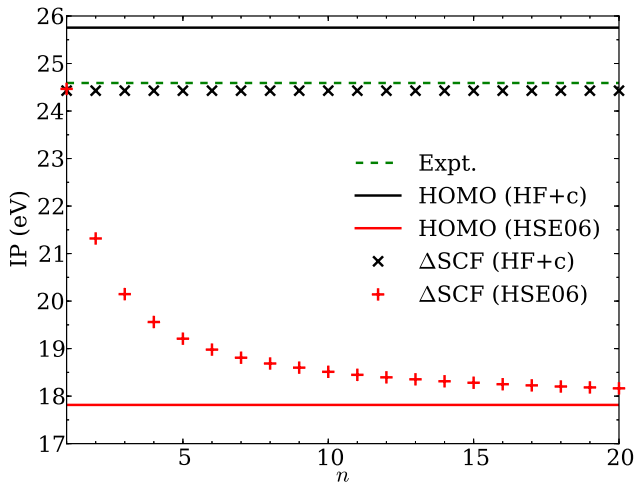


FIG. 5. IP of a dilute He_n cluster, comparing $-\epsilon_{\text{HOMO}}(\text{He}_n)$ to $E(\text{He}_n^+) - E(\text{He}_n)$ using the HSE06 functional and full Fock exchange with PBE correlation (HF+c), which correspond to the points (0.5, 0.25) and (0.0, 1.0) in HSE space. In HSE06, the ΔSCF and eigenvalue-based results converge for $n \rightarrow \infty$. The electron-hole of He_n^+ is localized on one atom with HF+c and uniformly divided among all n atoms with HSE06. Any n -dependence is a size-consistency error.

should also occur for localized defect states in crystals, but with the discrepancy in polarization reduced by ϵ_0^{-1} . Another solution is to include long-range Fock exchange to model the correct asymptotic of W , with its range parameters tuned to model the size of the molecule and approximately satisfy Koopmans’ theorem⁵⁰. Given our results with HSE, caution must be exercised when tuning range-separated hybrid functionals into a regime where HOMO and ΔSCF values of the IP match, because this may degrade the accuracy of other physical properties.

D. Conformational tests: BH42/04 barrier heights, T-96R bond lengths, and SC/40 lattice constants

The final set of tests are based on atomic conformations that are less pronounced than full formation, which leads to less variation of error in HSE space than the formation energies in Fig. (3). For the barrier heights in Fig. (6a), the optimal ω value at $a = 1$ is consistent with previous results¹³. The error trend in molecular bond lengths in Fig. (6b) matches well with molecular formation energies in Fig. (3). The increased $\tilde{\omega}$ -dependence at small $\tilde{\omega}$ and large a of the lattice constants in Fig. (6c) are the result of unconverged Brillouin zone sampling of the long-range exchange tail. In all cases, the minimum in MAE closely corresponds to the zero of ME. The net effect is to reduce small systematic errors in PBE that overestimate bond lengths and lattice constants and underestimate barrier heights.

E. Outlook on method development

Our combined computational survey and analysis of HSE functional space suggests several new directions for method development with varying degrees of expected difficulty and efficacy. We have shown the approximate correspondence of sX-LDA to the HSE functional form. Given the limited performance of sX-LDA for properties other than band gaps⁸, we conclude that HSE is both conceptually and empirically superior because of its use of PBE instead of LDA for correlation and long-range exchange. Any benefit to the system-dependence of the sX-LDA screening length that is negligible for solids and ill-defined for molecules is offset by optimization of a system-independent HSE screening length. Within the HSE form, we can recommend new parameters that are modest improvements over HSE06. We base this on an aggregate error metric shown in Fig. (7),

$$\frac{1}{\# \text{ of tests}} \sum_i^{\text{tests}} \left(\frac{\text{MAE}_i(\tilde{\omega}, a)}{\min_{\tilde{\omega}', a'} \text{MAE}_i(\tilde{\omega}', a')} - 1 \right). \quad (13)$$

The eigenvalue-based tests are excluded because of their systematic bias. This metric puts emphasis on the more sensitive tests and is zero if the MAE of each test can be simultaneously minimized. The “HSE12” functional, with $\omega = 0.185 \text{ \AA}^{-1}$ and $a = 0.313$, optimizes accuracy by minimizing the metric. The “HSE12s” functional, with $\omega = 0.408 \text{ \AA}^{-1}$ and $a = 0.425$, minimizes screening length while preserving the accuracy of HSE06. HSE12s has half the screening length of HSE06, which can reduce computational costs in implementations that make use of spatial decay in short-range Fock exchange. A summary of functionals and their performance is given in Table II.

The reduced cost of HSE12s can be demonstrated by the relative speed-up of an example: bulk aluminum. In GAUSSIAN (using the basis from Ref. 51), the relative speed of HSE12s compared to HSE06 is 1.6. The cause of this improvement is exchange integral screening⁵¹. In VASP, the speed-up is 1.4. Here, the improvement comes from reduced Brillouin zone sampling of the sX term for HSE12s compared to HSE06²³, requiring $5 \times 5 \times 5$ points instead of $6 \times 6 \times 6$ to achieve equivalent convergence.

Further progress in increasing functional accuracy will require alterations of the HSE form. More complicated screening forms have been proposed⁵², which enable more realistic W models, such as in Eq. (9), and may help to align the optimal choice of screening for multiple physical properties. The PBE model was designed for exclusively semilocal treatment of exchange, and a recent result⁵³ shows the benefits of refitting PBE dependent on how exchange is split into Fock and semilocal components, because it enables a fit of PBE to the residual, rather than total, exchange energy. Based on the strong ties between HSE and COHSEX outlined in this paper, it may be worthwhile to pursue semilocal DFT functionals based on a sX/Coulomb-hole partition⁵⁴ instead of an exchange/correlation partition. Given the observed error

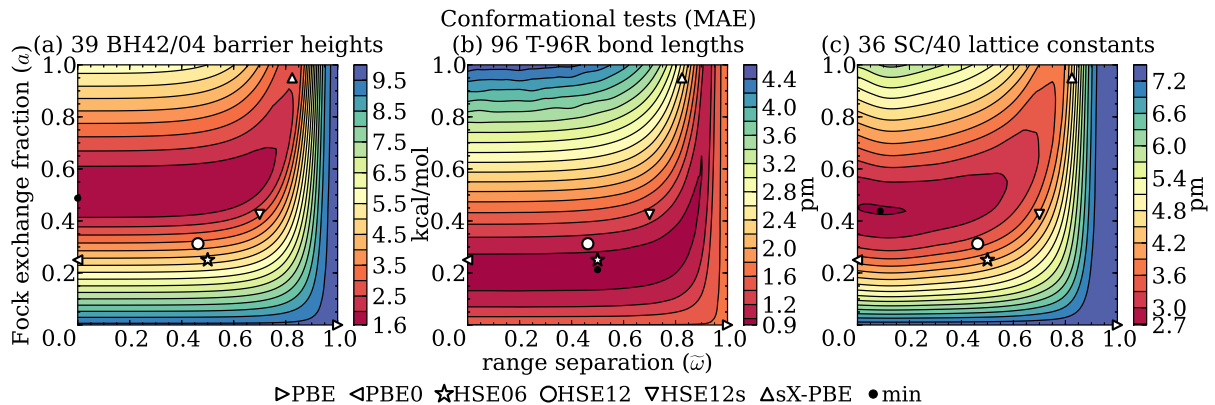


FIG. 6. Binary reaction barrier height, molecular bond length, and semiconductor lattice constant errors in HSE space.

trends in HSE space, it may be possible to construct a semilocal sX functional by taking the subset of accurate functionals to the $(\omega, a) \rightarrow \infty$ limit. Unfortunately, these suggestions are not likely to fix the large errors in HSE HOMO/LUMO eigenvalues for molecules, because they do not introduce any nonlocal screening effects.

The inevitability of nonlocality can be argued in the context of GKS theory as an approximation to COHSEX theory. The screened exchange operator in Eq. (8) is a direct product of ρ and W , which is a spatially localized operator for basic electronic phases. In an insulator⁵⁵, ρ decays exponentially with increasing $|\mathbf{r} - \mathbf{r}'|$, while W decays only algebraically. In a metal, it is ρ that decays algebraically and W that decays exponentially. In either case, the product is localized by one constituent while the other builds nonlocal dependence into the quantitative details. Hypothetical examples of nonlocal dependence are electron interference in ρ resulting from proximity to a scatterer in a metal or increased screening in W from proximity to a highly polarizable object in an insulator. In the context of DFT, the exchange-correlation hole is observed to be spatially localized, but no limits have been placed on its sensitivity to distant perturbations⁵⁶.

DFT modeling can be roughly split between quantities that are tractable (albeit expensive) to compute exactly (e.g. Fock exchange energy) and those that cannot be generally computed (e.g. exact correlation energy). At the level of COHSEX theory, W is contained within the first category and can be explicitly constructed from an independent-electron response function,

$$\chi_{\sigma,\sigma'}^0(\mathbf{r}, \mathbf{r}') = \sum_{i,j} \frac{f_i - f_j}{\epsilon_i - \epsilon_j} \psi_{i,\sigma}^*(\mathbf{r}) \psi_{j,\sigma}(\mathbf{r}) \psi_{j,\sigma'}^*(\mathbf{r}') \psi_{i,\sigma'}(\mathbf{r}')$$

$$W_{\sigma,\sigma'}^{-1}(\mathbf{r}, \mathbf{r}') = \left[\frac{1}{|\mathbf{r} - \mathbf{r}'|} \right]^{-1} - \chi_{\sigma,\sigma'}^0(\mathbf{r}, \mathbf{r}'), \quad (14)$$

for orbitals ψ_i , energies ϵ_i , and occupations f_i , and where \langle^{-1} , refers to operator inversion. Using such forms for W , promising results for total energies and charge excitations have been demonstrated for self-consistent quasiparticle methods⁵⁷⁻⁵⁹ and much of this accuracy is preserved by

the COHSEX approximation⁶⁰. It is conceivable that the precision and reliability necessary to attain the goal of “chemical accuracy” will only be achieved with a detailed treatment of W in the same way orbital-free DFT has not been able to achieve a level of accuracy comparable to methods containing the details of electronic orbitals⁶¹. The construction of ρ from electronic orbitals,

$$\rho_{\sigma,\sigma'}(\mathbf{r}, \mathbf{r}') = \sum_i f_i \psi_{i,\sigma}(\mathbf{r}) \psi_{i,\sigma'}^*(\mathbf{r}'), \quad (15)$$

contains its essential nonlocal character and accounts for much of the success of Kohn-Sham DFT. In principle, ρ and W have equal importance in COHSEX theory, and putting this into practice in COHSEX-inspired DFT functionals will require the use of Eq. (14).

The form of W in Eq. (14) highlights an open problem in self-consistent quasiparticle theory. Quasiparticle and GKS methods are designed to model charge excitations, but the electronic polarizability represented in Eq. (14) is supposed to arise from neutral excitations. The use of quasiparticle energies in Eq. (14) produces a systematic overestimate of band gaps, which has been removed with vertex corrections encoding electron-hole interactions⁶². Otherwise, the non-self-consistent evaluation of Eq. (14) using DFT methods is found to produce accurate mean-field models of static polarization⁶³. Similar observations have been made for HSE: that it approximates the optical gap rather than the charge gap when there is a significant difference between the two⁶⁴, even though it is a GKS theory that should be approximating the charge gap. A heuristic explanation for this effect is that the universal lack of exchange screening in HSE can be attributed to electrons (holes) being screened by both a ground-state polarization and an excess hole (electron). Just as with the excess polarization argument in section III C, this energy can be removed from the eigenvalues to improve their correspondence to quasiparticles, and in this case it can be re-identified for $\epsilon_{\text{LUMO}}^{\text{HSE}} - \epsilon_{\text{HOMO}}^{\text{HSE}}$ as the Coulomb binding energy between an electron and hole. It may be possible for a self-consistent COHSEX-based theory to avoid vertex corrections if it can define a consistent pair

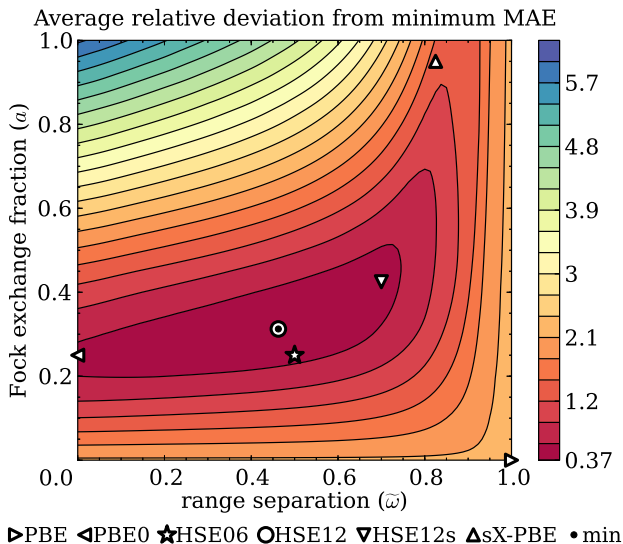


FIG. 7. Aggregate error in HSE space. The minimum of this error metric occurs at the HSE12 parameterization. HSE06 and HSE12s lie on a contour of equal error.

of mean fields: a polarization mean field, meant to model neutral excitations for Eq. (14), and a quasiparticle mean field containing the COHSEX self-energy from Eq. (8). Based on existing theory, it is possible to construct GKS and optimized effective potential (OEP)⁶⁵ methods from the same COHSEX-based total energy functional, with the GKS form serving as the quasiparticle theory and the OEP form serving as the polarization model. However, a consistent theoretical framework for such a “double” mean-field theory does not yet exist. The theory would need to specify the interrelations between the orbitals and energies of the two mean fields and how they should be used in concert to calculate a total electronic energy.

IV. CONCLUSIONS

The novelty of our study comes from HSE’s precarious perch between empirical and non-empirical DFT, with just two tunable parameters. This enables a thorough sampling of parameter space, similar to recent studies on the PBE functional⁶⁶. Besides the immediate benefit of further fine-tuning accuracy, the study reveals error trends supporting a connection between the HSE form and quasiparticle theory, which explains its success in approximating semiconductor band gaps. The degree to which multiple physical properties can be simultaneously optimized by a common set of parameters is pleasantly surprising. Unpleasant and unsurprising⁸ are the large discrepancies between Δ SCF and eigenvalue estimates of small molecule IPs and EAs, which we argue to originate from the absence of environment-dependent screening in the HSE functional resulting from discrepancies between W^{HSE} in Eq. (10) and W in Eq. (14). It is encouraging

TABLE II. Summary of important functionals in HSE space and their performance on various tests discussed in this paper.

Tests		PBE	PBE0	HSE06	HSE12	HSE12s
SC/40	ME	-1.13	0.39	-0.24	0.06	-0.16
band	MAE	1.13	0.44	0.32	0.23	0.28
gaps	RMSE	1.25	0.49	0.41	0.31	0.36
(eV)	max	-2.46	1.00	-0.90	-0.66	-0.95
G3/99	ME	-19.0	-2.6	-2.6	1.4	6.2
formation	MAE	19.6	5.2	5.2	4.8	7.3
energies	RMSE	24.0	7.4	7.4	6.7	10.1
(kcal/mol)	max	-72.0	-29.8	-30.0	26.3	40.7
G3/99	ME	-0.07	-0.05	-0.05	-0.05	-0.06
ionization	MAE	0.21	0.20	0.20	0.20	0.22
potentials	RMSE	0.28	0.28	0.29	0.30	0.32
(eV)	max	1.13	1.72	1.71	1.86	2.01
G3/99	ME	0.08	-0.01	-0.02	-0.04	-0.07
electron	MAE	0.13	0.17	0.17	0.19	0.22
affinities	RMSE	0.18	0.23	0.23	0.26	0.30
(eV)	max	0.78	1.08	1.07	1.14	1.20
BH42/04	ME	-9.6	-4.6	-4.8	-3.6	-2.9
barrier	MAE	9.6	4.6	4.8	3.7	2.9
heights	RMSE	10.3	4.9	5.0	3.9	3.2
(kcal/mol)	max	-20.0	-7.5	-7.7	-6.4	-5.9
T-96R	ME	1.6	0.0	0.0	-0.4	-0.7
bond	MAE	1.6	1.0	0.9	1.1	1.3
lengths	RMSE	1.9	1.5	1.4	1.7	1.9
(pm)	max	5.5	6.5	5.6	7.9	-7.1
SC/40	ME	7.4	3.1	3.5	2.6	2.9
lattice	MAE	7.4	3.7	4.1	3.5	3.9
constants	RMSE	8.5	4.5	4.9	4.2	4.7
(pm)	max	16.2	10.1	10.8	9.5	10.4

that this error can be fixed by correcting the long-range tail of W ⁵⁰. However, this simple fix is not transferrable to more complicated systems such as a molecule near a metal surface, where a model W such as Eq. (9) is not flexible enough to set $\varepsilon_0^{-1} = 0$ for the metal half-space and $\varepsilon_0^{-1} = 1$ for the empty half-space. There is much to be gained from incorporating more sophisticated models of W into the screened Fock exchange component of GKS functionals, such as Eq. (14) or a reasonable facsimile thereof⁶⁷.

ACKNOWLEDGMENTS

Sandia National Laboratories is a multi-program laboratory managed and operated by Sandia Corporation, a wholly owned subsidiary of Lockheed Martin Corporation, for the U.S. Department of Energy’s National Nuclear Security Administration under contract DE-AC04-94AL85000.

JRC and JEM wish to acknowledge support from the

National Science Foundation under grants No. DMR-0941645 and OCI-1047997 and the Department of Energy under grant No. DE-FG02-06ER46286. The computational resources used for this work were provided by the National Energy Research Scientific Computing Center (NERSC).

JEM thanks Norm Tubman, Leeor Kronik, and John Aidun for useful discussions related to this work.

- ¹J. P. Perdew, K. Burke, and M. Ernzerhof, *Phys. Rev. Lett.* **77**, 3865 (1996).
- ²C. Adamo and V. Barone, *J. Chem. Phys.* **110**, 6158 (1999).
- ³J. Heyd, G. E. Scuseria, and M. Ernzerhof, *J. Chem. Phys.* **118**, 8207 (2003).
- ⁴J. Paier, M. Marsman, and G. Kresse, *J. Chem. Phys.* **127**, 024103 (2007).
- ⁵A. Seidl, A. Görling, P. Vogl, J. A. Majewski, and M. Levy, *Phys. Rev. B* **53**, 3764 (1996).
- ⁶J. Heyd, J. E. Peralta, G. E. Scuseria, and R. L. Martin, *J. Chem. Phys.* **123**, 174101 (2005), band gap calculations are performed on experimental structures. Internal parameters for hexagonal structures are not specified in the SC/40 set, and we use experimental values^{68,69} of $u = 0.3821$ for AlN, $u = 0.3789$ for GaN, and $u = 0.3769$ for InN.
- ⁷M. A. L. Marques, J. Vidal, M. J. T. Oliveira, L. Reining, and S. Botti, *Phys. Rev. B* **83**, 035119 (2011).
- ⁸X. Zheng, A. J. Cohen, P. Mori-Sánchez, X. Hu, and W. Yang, *Phys. Rev. Lett.* **107**, 026403 (2011).
- ⁹A. Biller, I. Tamblyn, J. B. Neaton, and L. Kronik, *J. Chem. Phys.* **135**, 164706 (2011).
- ¹⁰M. Jain, J. R. Chelikowsky, and S. G. Louie, *Phys. Rev. Lett.* **107**, 216806 (2011).
- ¹¹M. Ernzerhof and J. P. Perdew, *J. Chem. Phys.* **109**, 3313 (1998).
- ¹²A. V. Krūkau, O. A. Vydrov, A. F. Izmaylov, and G. E. Scuseria, *J. Chem. Phys.* **125**, 224106 (2006).
- ¹³O. A. Vydrov, J. Heyd, A. V. Krūkau, and G. E. Scuseria, *J. Chem. Phys.* **125**, 074106 (2006).
- ¹⁴D. M. Bylander and L. Kleinman, *Phys. Rev. B* **41**, 7868 (1990).
- ¹⁵L. Hedin, *Phys. Rev.* **139**, A796 (1965).
- ¹⁶GAUSSIAN 09, Revision B.01, M. J. Frisch, G. W. Trucks, H. B. Schlegel, G. E. Scuseria, M. A. Robb, J. R. Cheeseman, G. Scalmani, V. Barone, B. Mennucci, G. A. Petersson, H. Nakatsuji, M. Caricato, X. Li, H. P. Hratchian, A. F. Izmaylov, J. Bloino, G. Zheng, J. L. Sonnenberg, M. Hada, M. Ehara, K. Toyota, R. Fukuda, J. Hasegawa, M. Ishida, T. Nakajima, Y. Honda, O. Kitao, H. Nakai, T. Vreven, J. A. Montgomery, Jr., J. E. Peralta, F. Ogliaro, M. Bearpark, J. J. Heyd, E. Brothers, K. N. Kudin, V. N. Staroverov, T. Keith, R. Kobayashi, J. Normand, K. Raghavachari, A. Rendell, J. C. Burant, S. S. Iyengar, J. Tomasi, M. Cossi, N. Rega, J. M. Millam, M. Klene, J. E. Knox, J. B. Cross, V. Bakken, C. Adamo, J. Jaramillo, R. Gomperts, R. E. Stratmann, O. Yazyev, A. J. Austin, R. Cammi, C. Pomelli, J. W. Ochterski, R. L. Martin, K. Morokuma, V. G. Zakrzewski, G. A. Voth, P. Salvador, J. J. Dannenberg, S. Dapprich, A. D. Daniels, O. Farkas, J. B. Foresman, J. V. Ortiz, J. Cioslowski, and D. J. Fox, Gaussian, Inc., Wallingford CT, 2010.
- ¹⁷G. Kresse and J. Hafner, *Phys. Rev. B* **47**, 558 (1993).
- ¹⁸G. Kresse and J. Hafner, *Phys. Rev. B* **49**, 14251 (1994).
- ¹⁹G. Kresse and J. Furthmüller, *Comput. Mat. Sci.* **6**, 15 (1996).
- ²⁰G. Kresse and J. Furthmüller, *Phys. Rev. B* **54**, 11169 (1996).
- ²¹See attached Supplemental Material for tabulated computational results and VASP 5.2 sX-LDA source patch.
- ²²G. Kresse and D. Joubert, *Phys. Rev. B* **59**, 1758 (1999).
- ²³J. Paier, M. Marsman, K. Hummer, G. Kresse, I. C. Gerber, and J. G. Ángyán, *J. Chem. Phys.* **124**, 154709 (2006).
- ²⁴F. Tran, *Phys. Lett. A* **376**, 879 (2012), reference orbitals are defined by the downsampled screened hybrid functional rather than semilocal DFT.
- ²⁵L. A. Curtiss, K. Raghavachari, P. C. Redfern, V. Rassolov, and J. A. Pople, *J. Chem. Phys.* **109**, 7764 (1998).
- ²⁶L. A. Curtiss, K. Raghavachari, P. C. Redfern, and J. A. Pople, *J. Chem. Phys.* **112**, 7374 (2000), relaxed structures and enthalpy corrections to separate out the electronic formation energy are calculated to the standards of G3 theory²⁵.
- ²⁷Y. Zhao and D. G. Truhlar, *J. Phys. Chem. A* **108**, 6908 (2004), molecular geometries are available at http://t1.chem.umn.edu/misc/database_group/database_therm_bh/.
- ²⁸V. N. Staroverov, G. E. Scuseria, J. Tao, and J. P. Perdew, *J. Chem. Phys.* **119**, 12129 (2003).
- ²⁹R. Asahi, W. Mannstadt, and A. J. Freeman, *Phys. Rev. B* **59**, 7486 (1999).
- ³⁰B. Lee, L.-W. Wang, C. D. Spataru, and S. G. Louie, *Phys. Rev. B* **76**, 245114 (2007).
- ³¹S. J. Clark and J. Robertson, *Phys. Rev. B* **82**, 085208 (2010).
- ³²R. Gómez-Abal, X. Li, M. Scheffler, and C. Ambrosch-Draxl, *Phys. Rev. Lett.* **101**, 106404 (2008).
- ³³J. Paier, R. Hirschl, M. Marsman, and G. Kresse, *J. Chem. Phys.* **122**, 234102 (2005).
- ³⁴J. P. Perdew and M. Levy, *Phys. Rev. Lett.* **51**, 1884 (1983).
- ³⁵S. T. Pantelides, D. J. Mickish, and A. B. Kunz, *Phys. Rev. B* **10**, 2602 (1974).
- ³⁶T. L. Gilbert, *Phys. Rev. B* **12**, 2111 (1975).
- ³⁷N. N. Lathiotakis, *Int. J. Quantum Chem.* (2012), DOI: 10.1002/qua.24069.
- ³⁸R. Resta, *Phys. Rev. B* **16**, 2717 (1977).
- ³⁹W. Jost, *J. Chem. Phys.* **1**, 466 (1933).
- ⁴⁰A. Görling and M. Ernzerhof, *Phys. Rev. A* **51**, 4501 (1995).
- ⁴¹R. D. Adamson, J. P. Dombroski, and P. M. Gill, *Chem. Phys. Lett.* **254**, 329 (1996).
- ⁴²A. Görling, *Phys. Rev. Lett.* **83**, 5459 (1999).
- ⁴³S. Ismail-Beigi, *Phys. Rev. B* **81**, 195126 (2010).
- ⁴⁴P. Sánchez-Friera and R. W. Godby, *Phys. Rev. Lett.* **85**, 5611 (2000).
- ⁴⁵P. Mori-Sánchez, A. J. Cohen, and W. Yang, *Phys. Rev. Lett.* **100**, 146401 (2008).
- ⁴⁶A. Savin, *Chem. Phys.* **356**, 91 (2009).
- ⁴⁷P. A. Schultz, *Phys. Rev. Lett.* **96**, 246401 (2006).
- ⁴⁸T. Koopmans, *Physica* **1**, 104 (1934).
- ⁴⁹We use the default PCM implementation in GAUSSIAN 09, with the polarization cavity defined by the intersection of atomic spheres with van der Waals radii. The dielectric model is set to $\epsilon_0 = \epsilon_\infty \rightarrow \infty$. PCM calculations are performed with the PBE functional and results are assumed to be transferrable to all HSE functionals.
- ⁵⁰T. Stein, H. Eisenberg, L. Kronik, and R. Baer, *Phys. Rev. Lett.* **105**, 266802 (2010).
- ⁵¹J. Heyd and G. E. Scuseria, *J. Chem. Phys.* **121**, 1187 (2004).
- ⁵²T. M. Henderson, A. F. Izmaylov, G. E. Scuseria, and A. Savin, *J. Chem. Phys.* **127**, 221103 (2007).
- ⁵³J. M. del Campo, J. L. Gázquez, S. B. Trickey, and A. Vela, *J. Chem. Phys.* **136**, 104108 (2012).
- ⁵⁴R. Armiento and A. E. Mattsson, *Phys. Rev. B* **68**, 245120 (2003).
- ⁵⁵W. Kohn, *Phys. Rev. Lett.* **76**, 3168 (1996).
- ⁵⁶G. Ortiz, I. Souza, and R. M. Martin, *Phys. Rev. Lett.* **80**, 353 (1998).
- ⁵⁷M. van Schilfgaarde, T. Kotani, and S. Faleev, *Phys. Rev. Lett.* **96**, 226402 (2006).
- ⁵⁸A. Kutepov, S. Y. Savrasov, and G. Kotliar, *Phys. Rev. B* **80**, 041103(R) (2009).
- ⁵⁹A. Stan, N. E. Dahlen, and R. van Leeuwen, *J. Chem. Phys.* **130**, 114105 (2009).
- ⁶⁰F. Bruneval, N. Vast, and L. Reining, *Phys. Rev. B* **74**, 045102 (2006).
- ⁶¹S. B. Trickey, V. V. Karasiev, and A. Vela, *Phys. Rev. B* **84**, 075146 (2011).
- ⁶²M. Shishkin, M. Marsman, and G. Kresse, *Phys. Rev. Lett.* **99**, 246403 (2007).
- ⁶³M. Shishkin and G. Kresse, *Phys. Rev. B* **75**, 235102 (2007).

- ⁶⁴E. N. Brothers, A. F. Izmaylov, J. O. Normand, V. Barone, and G. E. Scuseria, *J. Chem. Phys.* **129**, 011102 (2008).
- ⁶⁵S. Kümmel and L. Kronik, *Rev. Mod. Phys.* **80**, 3 (2008).
- ⁶⁶E. Fabiano, L. A. Constantin, and F. D. Sala, *J. Chem. Theory Comput.* **7**, 3548 (2011).
- ⁶⁷T. Gould and J. F. Dobson, *Phys. Rev. B* **84**, 241108(R) (2011).
- ⁶⁸H. Schulz and K. H. Thiermann, *Solid State Commun.* **23**, 815 (1977).
- ⁶⁹W. Paszkowicz, R. Černý, and S. Krukowski, *Powder Diffr.* **18**, 114 (2003).